6-2019

# Electromagnetic Analysis of a Wind Turbine Magnetic Gearbox

Kang Li
*University of North Carolina at Charlotte*

Sina Modaresahmadi
*University of North Carolina at Charlotte*

Wesley B. Williams
*University of North Carolina at Charlotte*

Jonathan Bird
*Portland State University*, bird@pdx.edu



## Citation Details

Li, K., Modaresahmadi, S., Williams, W., & Bird, J. Z. (2019). Electromagnetic analysis of a wind turbine magnetic gearbox. The Journal of Engineering, 2019(17), 4101-4105.

The Journal of Engineering

*The 9th International Conference on Power Electronics, Machines and Drives (PEMD 2018)*

IET Journals
The Institution of Engineering and Technology

# Electromagnetic analysis of a wind turbine magnetic gearbox

eISSN 2051-3305
Received on 20th June 2018
Accepted on 27th July 2018
doi: 10.1049/joe.2018.8006
www.ietdl.org

*Kang Li[1], Sina Modaresahmadi[2], Wesley Williams[2], Jonathan Z. Bird[1,3]* ✉

[1]*Department of Electrical and Computer Engineering, University of North Carolina at Charlotte, 9201 University, City Boulevard, Charlotte, NC, 28223, USA*

[2]*Department of Engineering Technology, University of North Carolina at Charlotte, 9201 University, City Boulevard, Charlotte, NC, 28223, USA*

[3]*Laboratory for Electromechanical Energy Conversion and Control, Department of Electrical and Computer Engineering, Portland State University, 1900 SW 4th Avenue, Portland, OR, 97201, USA*

✉ *E-mail: jonathan.bird@ieee.org*

**Abstract:** The design of the second stage of a 59:1 multi-stage magnetic gearbox for a wind turbine demonstrator is presented. The multi-stage series-connected magnetic gearbox is composed of a 6.45 first stage and 9.14 second stage. A flux-focusing spoke-type rotor typology is used with a unique segmented fully laminated design. The impact of structural design changes is considered with respect to torque density. A new rotor typology is presented that enables the magnetic gearbox to be mechanically assembled first without magnets.

## 1 Introduction

The most popular approach to converting the wind turbine's low-speed rotary motion into electricity is to utilise a doubly fed induction generator (DFIG) coupled with a mechanical gearbox. Currently, a majority of high-power wind turbines use this approach because the DFIG is of low cost and the power electronic converter typically only needs to be sized to around 30% of rated power [1–3]. Unfortunately, wind turbine gearboxes have been one of the main causes of wind turbine down time [4], and the gearbox failure rates increase with the power level [4, 5]. This has resulted in the wind turbine gearboxes not being able to achieve their desired 20 year design life [4, 6]. Furthermore, DFIGs utilise brushes which require regular maintenance which is difficult and expensive in many of the remote wind turbine site locations.

One of the main alternatives to the DFIG is the direct-drive (DD) permanent magnet (PM) generator which removes the reliability concerns regarding brushes and the mechanical gearbox. However, the torque density of a DD-PM generator is thermally limited (by current) and, therefore, a PM generator does not normally achieve torque densities >50 Nm/L [7, 8]. For this reason, DD-PM generators become very large when scaled up in size and their low torque density results in the need for a massive quantity of rare-earth magnet material being used [9, 10]. The increased size of the drivetrain results in a significantly higher installation cost and, therefore, the system is then less cost-competitive when compared with more traditional non-renewable energy sources or with the DFIG [11].

Magnetically geared generators [12–19] have recently been proposed as a way of increasing the wind-turbine drivetrain reliability without increasing the drivetrain size and, therefore, the installation cost [18]. A magnetic gearbox (MG) enables speed amplification to be achieved without any mechanical contact, they do not require gear lubrication and they have inherent overload protection. As the losses are primarily frequency dependent, they also have the potential to operate at a high conversion efficiency over a large loading range.

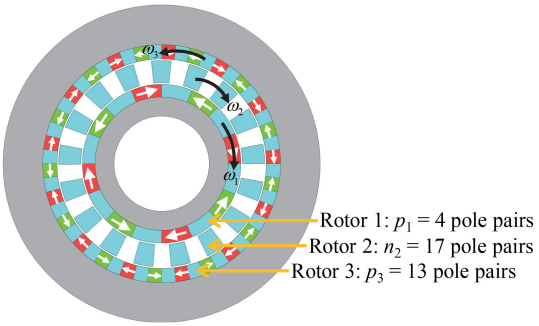


**Fig. 1** *Example of a coaxial flux-focusing magnetic gearbox*

The coaxial MG is the most studied typology [20–24]; an example of a flux-focusing coaxial MG typology is shown in Fig. 1. It consists of an inner rotor with $p_1$ pole pairs, an outer rotor with $p_3$ pole pairs, and a central rotor made of $n_2$ ferromagnetic segments, termed a cage rotor in this paper. In order to maximise torque, the pole combination must satisfy

$$n_2 = p_1 + p_3 \tag{1}$$

Then, the governing speed equation is given by [20]

$$n_2\omega_2 = p_1\omega_1 + p_3\omega_3 \tag{2}$$

If the outer rotor is held stationary, the torque is maximised. This results in a fixed speed ratio being created that is given by

$$\omega_1 = (n_2/p_1)\cdot\omega_2 \tag{3}$$

The use of an MG in a wind turbine has been studied by a number of authors [12–17, 19], and an outer stator [15, 17], inner stator [12], and central stator [16] integrated MG generator typology has been proposed for use in a wind turbine. Most analysis to date has focused on using a wind turbine gear ratio that is <10:1 [12–19]. To achieve gear ratios comparable to their mechanical counterparts used in wind turbines a multi-stage MG is required.

This paper follows on from the analysis work presented in [19] and focuses on the practical design analysis of the second stage of a 30 kW multi-stage series-connected MG wind turbine demonstrator. The gear ratio used for both stages is shown in Table 1, and an illustration of the two-stage design is shown in Fig. 2. The pole pair combination of the stage 2 MG was selected as $p_4 = 7$, $n_5 = 64$, and $p_6 = 57$. This gave a stage 2 gear ratio of $n_5/p_4 = 9.\overline{142857}$, and when connected in series to stage 1, the total gear ratio became 59:1.

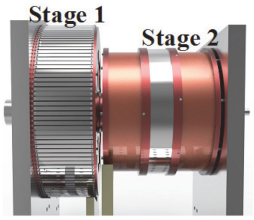


**Fig. 2** *Series-connected stage 1 and stage 2 magnetic gearbox*

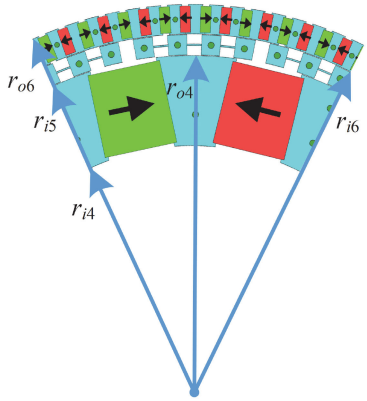


**Fig. 3** *Initial design of the stage 2 flux-focusing magnetic gearbox with a 0.5 mm air gap*

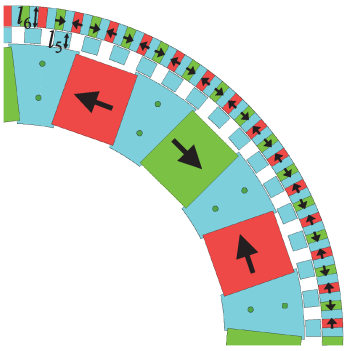


**Fig. 4** *Idealised stage 2 magnetic gearbox with a 1 mm air gap*

## 2 Initial magnetic gearbox design

An initial flux-focusing stage 2 MG design was developed. This design is shown in Fig. 3, and the design parameters are given in Table 2. Its design is based on the stage 1 design presented in [19]. In this initial design, the rotor air gaps were selected to be 0.5 mm. Using two-dimensional (2-D) finite element analysis (FEA), the calculated active region volumetric torque density and torque was computed to be 375 Nm/L and 2719 Nm, respectively. Serious deflection issues were encountered with the stage 1 laminated MG design. These deflection issues are discussed in [19]. Due to the mechanical issues encountered with the stage 1 design, a more robust structural design was sought for stage 2.

In the following sections, the design impact on the torque density of different structural design changes is presented. As the inner rotor does not experience significant radial deflection force [19], the inner rotor laminations and magnet design will be unchanged from what is shown in Fig. 3. Therefore $(r_{i4}, r_{o4}) = (155, 213)$ mm. This decision was made to reduce re-fabrication costs.

## 3 Ideal magnetic gearbox design

An ideal outer and a cage rotor typology were first considered in which the air gaps were increased to 1 mm; this design is shown in Fig. 4. The ideal design gives the upper torque capability limit for this typology. The air gap was increased in order to provide more tolerance robustness.

**Table 1** Gear ratios used for each stage of the coaxial magnetic gearbox

| | | |
|---|---|---|
| Stage 1 | inner rotor, $p_1$ | 11 |
| | cage rotor, $n_2$ | 71 |
| | outer rotor, $p_3$ | 60 |
| | gear ratio, $G_{12}$ | 6.45 |
| Stage 2 | inner rotor, $p_4$ | 7 |
| | cage rotor, $n_5$ | 64 |
| | outer rotor, $p_6$ | 57 |
| | gear ratio, $G_{45}$ | $9.\overline{142857}$ |
| Total gear ratio, $G_{12}G_{45}$ | | 59.012987 |

**Table 2** Geometric and material properties for the initial and final stage 2 magnetic gearbox design

| Description | | Initial value | Final value | Unit |
|---|---|---|---|---|
| inner rotor | inner radius, $r_{i4}$ | 155 | 155 | mm |
| | outer radius, $r_{o4}$ | 213 | 213 | mm |
| | radial magnet length | 54 | 54 | mm |
| | magnet width | 47.25 | 47.25 | mm |
| cage rotor | inner radius, $r_{i5}$ | 213.5 | 214 | mm |
| | outer radius, $r_{o5}$ | 226.5 | 226 | mm |
| outer rotor | inner radius, $r_{i6}$ | 227 | 227 | mm |
| | outer radius, $r_{o6}$ | 246 | 253.675 | mm |
| | radial magnet length | 17 | 17 | mm |
| | magnet width | 6.75 | 6.75 | mm |
| material | NMX-40CH, $B_m$ | 1.28 | 1.28 | T |
| | M19 conductivity | 0 | 0 | S/m |
| | steel rod 416 resistivity | 57 | 57 | μΩ cm |
| axial length, $d$ | | 38.1 | 38.1 | mm |
| air gap, $g$ | | 0.5 | 1 | mm |

To maximise torque density, a 2-D FEA torque density analysis was conducted in which the cage rotor and outer rotor radial lengths were varied whilst holding all other parameters constant. The cage rotor length is defined as

$$l_5 = r_{o5} - r_{i5} \tag{4}$$

and the outer rotor length is defined as

$$l_6 = r_{o6} - r_{i6} \tag{5}$$

The cage rotor length was varied from $l_5 = 7$ mm to $l_5 = 16$ mm at 1 mm intervals. The outer rotor length was also varied from $l_6 = 15$ mm to $l_6 = 35$ mm at 1 mm step intervals. The torque density analysis results for the 210 different 2-D FEA simulation cases is shown in Fig. 5. The equations used to compute the active region volumetric torque density is given by

$$T_{vd} = \frac{T_5}{\pi r_{o6}^2 d} \tag{6}$$

where $T_5$ is the torque on the low-speed cage rotor, $r_{o6}$ is the outer rotor radius, and $d$ is the axial stack length. The active region mass torque density was computed from

$$T_m = \frac{T_5}{m_m + m_s} \tag{7}$$

where $m_m$ is the magnet material mass and $m_s$ is lamination and support rod material mass. The radial length of the cage rotor, $l_5$, is shown in the legend of Fig. 5. Fig. 5 shows that a peak exists for maximising the volumetric torque density, and this is at the

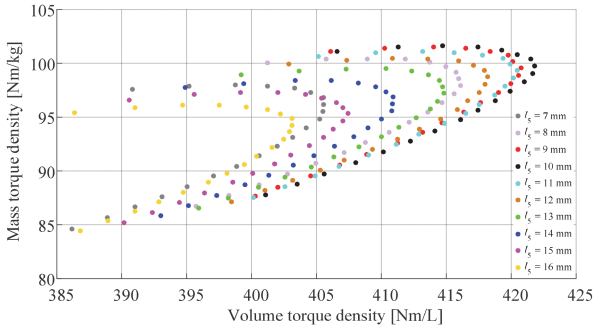


**Fig. 5** *Mass and volume torque density analysis plot when $l_5$ and $l_6$ were both varied for the idealised MG design*

**Table 3** 2-D calculated peak torque density at respective cage bar lengths

| $l_5$, mm | $l_6$, mm | Volume torque density, Nm/L | Mass torque density, Nm/kg |
|---|---|---|---|
| 7 | 21 | 405.5 | 96.8 |
| 8 | 23 | 416.1 | 97.9 |
| 9 | 22 | 420.7 | 99.6 |
| 10 | 22 | 421.8 | 99.8 |
| 11 | 22 | 420.5 | 99.4 |
| 12 | 22 | 418.2 | 98.7 |
| 13 | 23 | 414.8 | 97.2 |
| 14 | 22 | 410.9 | 96.9 |
| 15 | 23 | 407.4 | 95.3 |

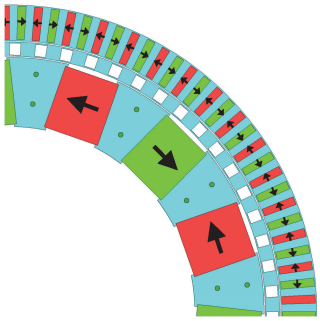

**Fig. 6** *Stage 2 MG with 1 mm bridges on the cage and outer rotors*

expense of a non-optimal mass torque density. Table 3 gives a summary of the peak torque density values for each cage bar length $l_5$. The peak volumetric torque density occurs when ($l_5$, $l_6$) = (10, 22) mm. In this analysis, the peak volumetric torque density is selected over mass torque density.

## 4 Magnetic gearbox with bridge supports

In order to make the MG have higher mechanical strength, a 1 mm bridge was added on both radial sides of the cage rotor and outer rotor as shown in Fig. 6. The radial lengths of the cage rotor and outer rotor were then again varied. The resultant torque density plot and results are shown in Fig. 7 and Table 4. The bridges introduce significant additional flux leakage, as shown in Fig. 8, and this greatly reduces the peak torque density. From studying Table 4, it can be noted that the peak volumetric torque density now is at ($l_5$, $l_6$) = (12, 24) mm.

## 5 Segmented bridge support design

In order to fabricate the laminated parts, the cage and outer rotors need to be segmented. The radial size is too large to be manufactured as a single contiguous piece. Using the segmented structure, as shown in Fig. 9, the analysis in Sections 3 and 4 was repeated. The sweep analysis results for all length combinations are

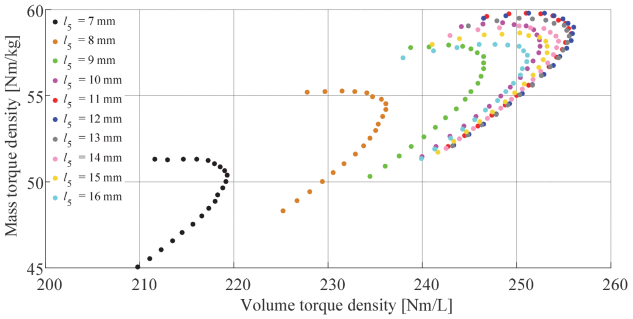


**Fig. 7** *Mass and volume torque density analysis plot when both $l_5$ and $l_6$ were varied for the MG bridge design. The length $l_6$ was varied from 17 to 37 mm at 1 mm intervals*

**Table 4** Peak torque density at respective cage bar lengths

| $l_5$, mm | $l_6$, mm | Volume torque density, Nm/L | Mass torque density, Nm/kg |
|---|---|---|---|
| 7 | 25 | 219.3 | 50.4 |
| 8 | 25 | 236.2 | 54.2 |
| 9 | 25 | 246.5 | 56.6 |
| 10 | 25 | 252.5 | 57.9 |
| 11 | 25 | 255.8 | 58.6 |
| 12 | 24 | 256.1 | 59.0 |
| 13 | 25 | 255.6 | 58.5 |
| 14 | 25 | 254.4 | 58.2 |
| 15 | 26 | 253.2 | 57.5 |

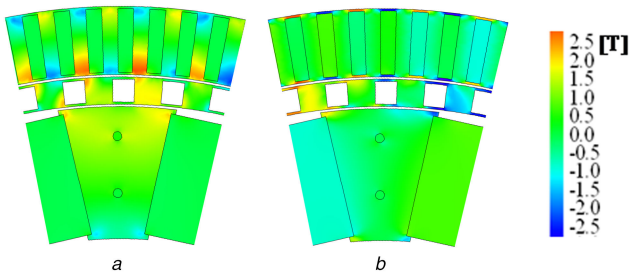


**Fig. 8** *Surface field plot for bridge support MG Design III showing* ***(a)*** Radial flux density $B_r$ and, ***(b)*** Azimuthal flux density $B\theta$ for the bridge support MG design when ($l_5$, $l_6$) = (12, 30) mm. The bridge leakage flux is clearly evident

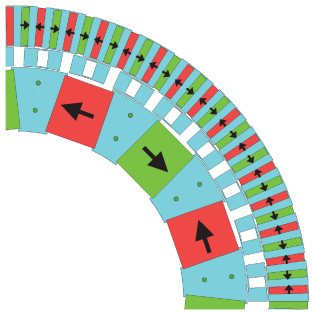

**Fig. 9** *Stage 2 magnetic gearbox with 1 mm bridges on the cage and outer rotors and segmented sections*

shown in Fig. 10. It can be noted that the peak torque density increases when compared to using bridges on all segments.

Fig. 11 shows the torque versus mass torque density and volume torque density for the segmented design. From Fig. 11, it can be noted that the peak torque density does not occur at the peak torque value. This is because higher torque values are only achieved when the outer rotor radius, $r_{o6}$, is increased. The peak volume torque density values for the different cage bar radial lengths, $l_5$, are summarised in Table 5.

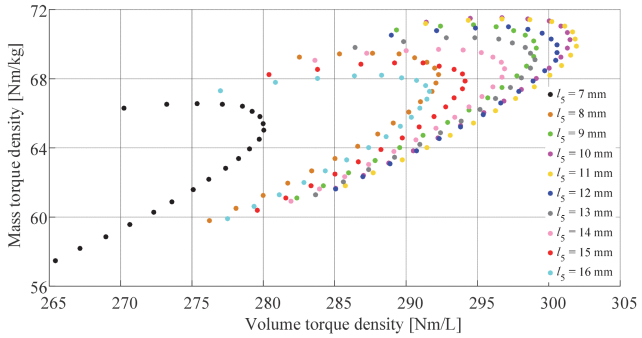


**Fig. 10** *Mass and volume torque density analysis plot when both $l_5$ and $l_6$ were varied for the segmented bridge design. The length $l_6$ was varied from 17 to 37 mm*

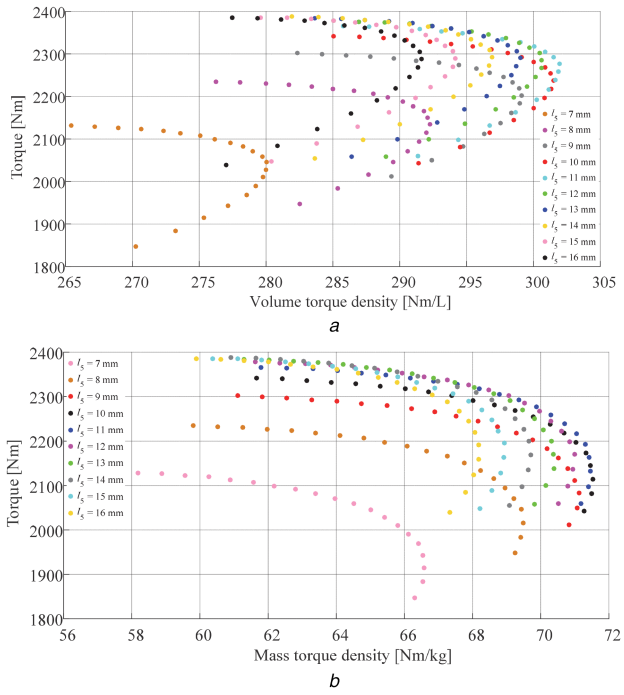


**Fig. 11** *Volumetric and Mass torque density sweep analysis showing*
***(a)*** Torque vs. volumetric torque density and, ***(b)*** Torque vs. mass torque density when both $l_5$ and $l_6$ were varied

**Table 5** Peak torque density at respective cage bar lengths

| $l_5$, mm | $l_6$, mm | Volume torque density, Nm/L | Mass torque density, Nm/kg |
|---|---|---|---|
| 7 | 25 | 280.0 | 65.0 |
| 8 | 24 | 292.2 | 68.2 |
| 9 | 24 | 299.1 | 69.7 |
| 10 | 24 | 301.4 | 70.2 |
| 11 | 25 | 301.9 | 69.8 |
| 12 | 24 | 300.5 | 69.9 |
| 13 | 25 | 299.0 | 69.1 |
| 14 | 25 | 296.8 | 68.5 |
| 15 | 25 | 294.1 | 67.8 |

## 6 Final magnetic gearbox design

The difficulties encountered during the re-assembly of the stage 1 design [19] lead to the invention of a new MG design approach in which the entire MG is first fully assembled without any magnets. Then following the successful testing of the mechanical design without magnets, the magnets can be inserted directly into the assembled rotor structure. This is similar to the approach taken when assembling interior PM motors [25]. Using this approach, the deflection during the assembly process can be minimised. With this

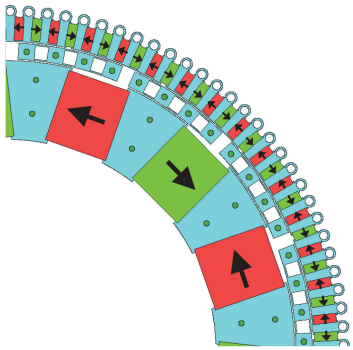

**Fig. 12** *Final design of the stage 2 MG*

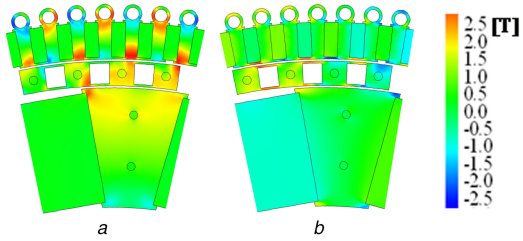


**Fig. 13** *Surface plot of the*
***(a)*** Radial magnetic flux density, $B_r$, and ***(b)*** Azimuthal magnetic flux density, $B_\theta$

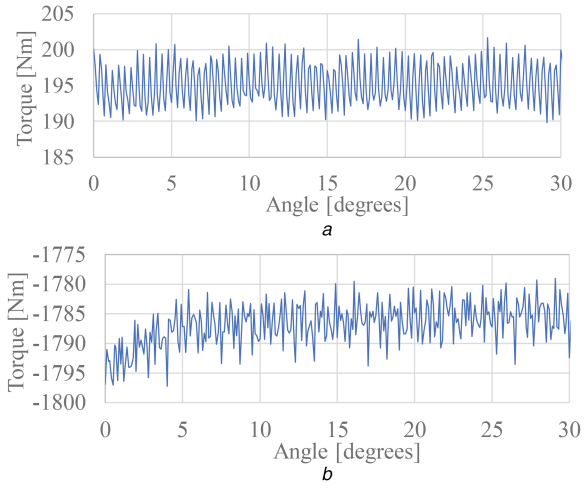


**Fig. 14** *Calculated 2-D transient FEA torque on the*
***(a)*** Inner rotor and, ***(b)*** Cage rotor when neglecting losses

design concept in mind, the outer rotor typology was modified to that shown in Fig. 12. The outer rotor is still supported by bridges on the inner radius like in the prior design. However, the outer rotor radius now has support holes for retaining rods but no bridges. This design change mitigates some of the outer leakage flux whilst still providing mechanical support to both sides of the outer rotor. Furthermore, it moves the outer rotor support rods away from the air gap, thereby significantly reducing eddy current losses. The reduction in outer radii leakage is evident in Fig. 13.

It should also be noted that in this final design, the outer rotor radial length was reduced to enable existing outer magnets to be used which have a length of $l_{om} = 17$ mm. A summary of the final MG design parameters is given in Table 2. The 2-D calculated volume and mass torque density are 232 Nm/L and 57 Nm/kg, respectively. The torque ripple is low as shown in Fig. 14. The mechanical assembly is shown in Figs. 15 and 16. The assembly steps will be primarily based on an axial layer-by-layer assembly process. This is possible because the magnets are axially segmented into five parts.

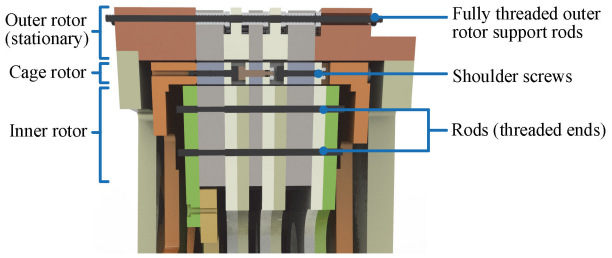


**Fig. 15** *Positioning of inner, cage, and outer rotors connecting components of stage 2 MG*

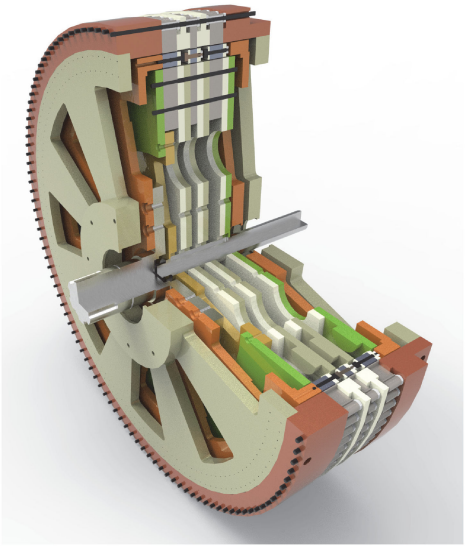

**Fig. 16** *90° cut-away view of the stage 2 MG showing all the interior mechanical components*

## 7 Conclusions

The electromagnetic FEA design analysis for the stage 2 part of a multi-stage MG has been presented. A new mechanical design was presented which allows the MG to be first assembled without inserting magnets. This helps to reduce the deflection during the assembly process. After adding additional necessary mechanical supports, the torque density has reduced significantly from the idealised design. The stage 2 MG torque density was calculated using 2-D FEA to be 232 Nm/L.

## 8 Acknowledgments

The authors would gratefully like to thank the JMAG Corporation and ANSYS Corporation for the use of their FEA software. This work was supported in part by the Department of Energy under grant DE-EE0006801 and in part by a North Carolina Ocean Energy grant.

## 9 References

[1] Muller, S., Deicke, M., Doncker, R.W.D.: 'Doubly fed induction generator systems for wind turbines', *IEEE Ind. Appl. Mag.*, 2002, **8**, (3), pp. 26–33

[2] Wang, F., Zhang, Y., Shen, Y.: 'Comparison of different structures for variable speed constant frequency wind power generation'. Int. Conf. Electricals Machines Systems, Wuhan, China, October 2008, pp. 2234–2238

[3] Li, H., Chen, Z.: 'Overview of different wind generator systems and their comparison', *IET Renew. Power Gener.*, 2008, **2**, (2), pp. 123–138

[4] Musial, W., Butterfield, S., McNiff, B.: 'Improving wind turbine gearbox reliability'. NREL/CP-500-41548, National Renewable Energy Laboratory, May 2007

[5] Sheng, S., Veers, P.: 'Wind turbine drivetrain condition monitoring – an overview'. Presented at the MFPT: Applied Systems Health Management Conf., Virginia Beach, VA, 10–12 May 2011

[6] Rensselar, J.V.: 'The elephant in the wind turbine', *Tribo. Lub. Tech.*, 2010, pp. 2–12

[7] Dubois, M.R.J.: 'Optimized permanent magnet generator topologies for direct-drive wind turbines'. PhD Thesis, Delft University of Technology, Delft, Netherlands, 2004

[8] Miller, T.J.E.: '*Brushless permanent-magnet and reluctance motor drives*' (Oxford University Press, Cary, 1989)

[9] Kasinathan, P., Grauers, A., Hamdi, E.S.: 'Force density limits in low-speed permanent-magnet machines due to saturation', *IEEE Trans. Energy Convers.*, 2005, **20**, (1), pp. 37–44

[10] Dorrell, D.G., Ngu, S.S., Cossar, C.: 'Comparison of high pole number ultra-low speed generator designs using slotted and air-gap windings', *IEEE Trans. Magn.*, 2012, **48**, (11), pp. 3120–3123

[11] Polinder, H., Van der Pijl, F.F.A., de Vilder, G.J., *et al.*: 'Comparison of direct-drive and geared generator concepts for wind turbines', *IEEE Trans. Energy Convers.*, 2006, **21**, (3), pp. 725–733

[12] Jian, L., Chau, K.T., Jiang, J.Z.: 'A magnetic-geared outer-rotor permanent-magnet brushless machine for wind power generation', *IEEE Trans. Ind. Appl.*, 2009, **45**, (3), pp. 954–962

[13] Frank, N.W., Toliyat, H.A.: 'Gearing ratios of a magnetic gear for wind turbines'. Presented at the IEEE Electric Machines Drive Conf., Miami, FL, 3–6 May 2009

[14] Desvaux, M., Latimier, R.L.G., Multon, B., *et al.*: 'Design and optimization of magnetic gears with arrangement and mechanical constraints for wind turbine applications'. Presented at the Eleventh Int. Conf. Ecological Vehicles Renewable Energies, Monaco, Monaco, April 2016

[15] Penzkofer, A.: 'Analytical modelling and analysis of magnetic gears and pseudo direct drives for large wind turbines'. PhD Thesis, Electrical and Computer Engineering, University of Sheffield, November 2016

[16] Jian, L., Xu, G., Gong, Y., *et al.*: 'Electromagnetic design and analysis of a novel magnetic-gear-integrated wind power generator using time-stepping finite element method', *Prog. Electromagn. Res.*, 2011, **113**, pp. 351–367

[17] Belkhir, K.S., Khenfer, N.: 'Magnetic gear generator for wind energy', *Prz. Elektrotech.*, 2013, **5**, pp. 72–75

[18] Wang, R., Gerber, S.: 'Magnetically geared wind generator technologies: opportunities and challenges', *Appl. Energy*, 2014, **136**, pp. 817–826

[19] Li, K., Wright, J., Modaresahmadi, S., *et al.*: 'Designing the first stage of a series connected multistage coaxial magnetic gearbox for a wind turbine demonstrator'. 9th IEEE Energy Conversion Congress Exposition, Cincinnati, USA, 1–5 October 2017, pp. 1247–1254

[20] Martin, T.B.: 'Magnetic transmission'. USA Patent # 3,378,710, 1968

[21] Rasmussen, P.O., Andersen, T.O., Jorgensen, F.T., *et al.*: 'Development of a high-performance magnetic gear', *IEEE Trans. Ind. Appl.*, 2005, **41**, (3), pp. 764–770

[22] Atallah, K., Calverley, S.D., Howe, D.: 'Design, analysis and realisation of a high-performance magnetic gear', *IEE Proc., Electr. Power Appl.*, 2004, **151**, (2), pp. 135–143

[23] Uppalapati, K.K., Bomela, W.B., Bird, J.Z., *et al.*: 'Experimental evaluation of low-speed flux-focusing magnetic gearboxes', *IEEE Trans. Ind. Appl.*, 2014, **50**, (6), pp. 3637–3643

[24] Som, D., Li, K., Kadel, J., *et al.*: 'Analysis and testing of a coaxial magnetic gearbox with flux concentration Halbach rotors', *IEEE Trans. Magn.*, 2017, **53**, (11), pp. 1–6

[25] Asano, Y., Shinto, M., Ito, H., *et al.*: 'Motor using a rotor including an interior permanent magnet'. USA Patent # 6,008,559, 1999